A Biophysically Based Mathematical Model for the Kinetics of Mitochondrial Calcium Uniporter

ARTICLE *in* BIOPHYSICAL JOURNAL · MARCH 2009

Impact Factor: 3.97 · DOI: 10.1016/j.bpj.2008.11.005 · Source: PubMed

3 AUTHORS:

Ranjan Dash
Medical College of Wisconsin
79 PUBLICATIONS **945** CITATIONS
SEE PROFILE

Feng Qi
Sanford Burnham Prebys Medical Discovery …
27 PUBLICATIONS **435** CITATIONS
SEE PROFILE

Daniel Beard
Medical College of Wisconsin
138 PUBLICATIONS **3,240** CITATIONS
SEE PROFILE

A Biophysically Based Mathematical Model for the Kinetics of Mitochondrial Calcium Uniporter

Ranjan K. Dash, Feng Qi, and Daniel A. Beard*
Biotechnology and Bioengineering Center and Department of Physiology, Medical College of Wisconsin, Milwaukee, Wisconsin 53226

ABSTRACT Ca^{2+} transport through mitochondrial Ca^{2+} uniporter is the primary Ca^{2+} uptake mechanism in respiring mitochondria. Thus, the uniporter plays a key role in regulating mitochondrial Ca^{2+}. Despite the importance of mitochondrial Ca^{2+} to metabolic regulation and mitochondrial function, and to cell physiology and pathophysiology, the structure and composition of the uniporter functional unit and kinetic mechanisms associated with Ca^{2+} transport into mitochondria are still not well understood. In this study, based on available experimental data on the kinetics of Ca^{2+} transport via the uniporter, a mechanistic kinetic model of the uniporter is introduced. The model is thermodynamically balanced and satisfactorily describes a large number of independent data sets in the literature on initial or pseudo-steady-state influx rates of Ca^{2+} via the uniporter measured under a wide range of experimental conditions. The model is derived assuming a multi-state catalytic binding and Eyring's free-energy barrier theory-based transformation mechanisms associated with the carrier-mediated facilitated transport and electrodiffusion. The model is a great improvement over the previous theoretical models of mitochondrial Ca^{2+} uniporter in the literature in that it is thermodynamically balanced and matches a large number of independently published data sets on mitochondrial Ca^{2+} uptake. This theoretical model will be critical in developing mechanistic, integrated models of mitochondrial Ca^{2+} handling and bioenergetics which can be helpful in understanding the mechanisms by which Ca^{2+} plays a role in mediating signaling pathways and modulating mitochondrial energy metabolism.

INTRODUCTION

The Ca^{2+} ion has multiple roles in mitochondrial function and dysfunction. It is known to mediate signaling pathways between cytosol and mitochondria and modulate mitochondrial energy metabolism. Alteration of mitochondrial Ca^{2+} homeostasis can lead to mitochondrial dysfunction and cellular injury (1–8). Despite the importance of mitochondrial Ca^{2+} to metabolic regulation and mitochondrial bioenergetics, and to cell physiology and pathophysiology, there are still significant gaps in our understanding of the structure, composition, and kinetic properties of mitochondrial Ca^{2+} transport systems (e.g., Ca^{2+} uniporter).

Mitochondrial Ca^{2+} uniporter, located on the inner mitochondrial membrane (IMM), is the primary influx pathway for Ca^{2+} in energized (respiring) mitochondria, and hence is a key regulator of mitochondrial Ca^{2+} (1,6,7). This uniporter-mediated mitochondrial Ca^{2+} uptake is known to be inhibited by divalent cations (e.g., Mg^{2+}, Mn^{2+}) and protons (H^+) (e.g., see (9–14)). Although the uptake of Ca^{2+} through the uniporter in respiring mitochondria has been extensively studied experimentally since the late 1960s, the kinetics of Ca^{2+} uptake has not been well characterized in terms of a mechanistic model that accounts for the thermodynamics of the transport process and other physiochemical mechanisms such as allosteric cooperative binding of Ca^{2+} to the uniporter and competitive binding and inhibition by other cations (e.g., Mg^{2+}, H^+). In fact, there is no mechanistic theoretical model of the uniporter in the literature that is thermodynamically feasible and satisfactorily describes independently published data sets on Ca^{2+} fluxes via the uniporter measured under a wide range of experimental conditions. Our recently published model of the uniporter (15) that is thermodynamically balanced and fits a large set of data incorporates a phenomenological factor that is not biophysically mechanistic. The need for such a mechanistic, credible and validated model of the uniporter is apparent in developing computer simulations of mitochondrial Ca^{2+} uptake and forming the basis for constructing biophysically-based, integrated models of mitochondrial Ca^{2+} handling and bioenergetics, which can be helpful in understanding the mechanisms by which Ca^{2+} plays a role in mediating signaling pathways and modulating mitochondrial energy metabolism (15).

Magnus and Keizer (16,17) developed a model of mitochondrial Ca^{2+} uniporter as a module of an integrated model of mitochondrial energy metabolism and Ca^{2+} handling to understand the direct effects of mitochondrial Ca^{2+} on ATP production in pancreatic β-cells. The kinetic model of the uniporter was based on a hypothetical four-state allosteric binding mechanism of Ca^{2+} to the uniporter and the Goldman-Hodgkin-Katz constant-field-type approximation for electrodiffusion and was parameterized using the experimental data of Gunter and co-workers (6,18) on Ca^{2+} uptake in isolated respiring mitochondria from rat liver. The Magnus-Keizer model was adopted by Cortassa et al. (19) in their integrated model of cellular and mitochondrial energy metabolism and Ca^{2+} dynamics in cardiomyocytes. However, the Magnus-Keizer model of the uniporter has the limitation that the model collapses for membrane potential $\Delta\Psi \leq \Delta\Psi^* = 91$ mV, and

Submitted June 16, 2008, and accepted for publication November 5, 2008.

*Correspondence: dbeard@mcw.edu

Editor: Michael D. Stern.

0006-3495/09/02/1318/15 $2.00

doi: 10.1016/j.bpj.2008.11.005

is not thermodynamically balanced. In addition, the model does not fit to the earlier experimental data of Scarpa and co-workers (10,11) on Ca^{2+} uptake in isolated respiring mitochondria from rat liver and rat heart. Furthermore, the Magnus-Keizer integrated model of mitochondrial Ca^{2+} handling predicts a high steady-state mitochondrial [Ca^{2+}] (~15 μM) in response to a low cytoplasmic [Ca^{2+}] (~1 μM) which is uncharacteristic for cardiac cells (13,20).

Due to the limitations in the Magnus-Keizer model of mitochondrial Ca^{2+} handling, Jafri and co-workers (21,22) recently developed an integrated model of mitochondrial energy metabolism and Ca^{2+} dynamics to understand the role of Ca^{2+} in the regulation of NADH and ATP production in cardiac mitochondria. Their model of mitochondrial Ca^{2+} uniporter, which is based on the assumption that the uniporter is a highly permeable ion channel selective mostly to Ca^{2+}, describes the recent experimental observations of Kirichok et al. (23) on Ca^{2+} uptake and Ca^{2+} current through the uniporter obtained using patch-clamp techniques in mitoplasts obtained from cardiac mitochondria. However, their model does not fit to the experimental data of Scarpa and co-workers (10,11) and Gunter and co-workers (6,18).

In this work, we introduce a mechanistic mathematical model of mitochondrial Ca^{2+} uniporter that extends and provides the biophysical basis for our recently developed model of the uniporter (15). This model is thermodynamically balanced and adequately describes the experimental data of Scarpa and co-workers (10,11) as well as Gunter and co-workers (6,18) on Ca^{2+} fluxes through the Ca^{2+} uniporter in respiring mitochondria isolated from rat heart and rat liver measured under a varieties of experimental conditions. The model is based on a combination of Michaelis-Menten kinetics for carrier-mediated facilitated transport (24,25) and Eyring's free-energy barrier theory for absolute reaction rates associated with electrodiffusion (25–28). Specifically, the model accounts for a possible mechanism that assumes allosteric cooperative binding of Ca^{2+} to the uniporter, as revealed in the experimental data of Scarpa and co-workers (10,11). In addition, the model satisfies the Ussing flux ratio (25,29), which specifies the relationship between overall forward and reverse fluxes in a thermodynamically feasible transport process across a biological membrane (30).

MATHEMATICAL FORMULATION

Experimental data for model development and validation

The structure and composition of mitochondrial Ca^{2+} uniporter and kinetic mechanism associated with mitochondrial Ca^{2+} transport via the uniporter are not well known. However, experimental data on the kinetics of mitochondrial Ca^{2+} uptake are available from the work of Scarpa and co-workers (10,11) and Gunter and co-workers (6,18). This data describes the extra-mitochondrial [Ca^{2+}] and mitochondrial membrane potential $\Delta\Psi$ dependencies of mitochondrial Ca^{2+} uptake, measured in respiring mitochondria isolated from rat heart and rat liver. The data of Scarpa and co-workers reveals the sigmoid nature of mitochondrial Ca^{2+} uptake when plotted against the extra-mitochondrial [Ca^{2+}], suggesting allosteric cooperative binding of at least two Ca^{2+} to the uniporter in the process of uniporter-mediated Ca^{2+} transport into mitochondria. The data of Gunter and co-workers reveals a nonlinear, non-Goldman-Hodgkin-Katz type of dependency of mitochondrial Ca^{2+} uptake on membrane potential $\Delta\Psi$. Our kinetic model of the uniporter that is developed here based on physical-chemical principles is parameterized to accurately reproduce the experimental data of Scarpa and co-workers as well as Gunter and co-workers.

Proposed mechanism for Ca^{2+} transport into mitochondria

In view of this available kinetic data, a multi-state catalytic binding and interconversion mechanism combined with Eyring's free-energy barrier theory for absolute reaction rates and electrodiffusion (25–28) is proposed to develop the mathematical model of Ca^{2+} transport via the mitochondrial Ca^{2+} uniporter. The proposed transport mechanism is schematized in Fig. 1. The uniporter is assumed to have two binding sites for Ca^{2+} and the binding sites are assumed to be exposed to either side of the IMM. An ionized free Ca^{2+} molecule from the cytoplasmic (external) side of the IMM first binds to the unbound uniporter (T) (State 1) to form the intermediate complex $T\,Ca_e^{2+}$ (State 2) which then favors binding of another ionized free Ca^{2+} molecule (cooperative binding) to form the ternary complex $T\,Ca_e^{2+}Ca_e^{2+}$ (State 5). The complex $T\,Ca_e^{2+}Ca_e^{2+}$ then undergoes conformal changes or flips upside down (Ca^{2+} translocation) to form the ternary complex $Ca_x^{2+}Ca_x^{2+}T$ (State 6). The complex $Ca_x^{2+}Ca_x^{2+}T$ in the matrix (internal) side of the IMM goes through the reverse process where it dissociates in two steps to form the intermediate complex $Ca_x^{2+}\,T$ (State 3), unbound uniporter (T) (State 1), and ionized free Ca^{2+}. The proposed transport scheme also assumes possible cross-interactions between the uniporter, external Ca^{2+}, and internal Ca^{2+} to form the intermediate ternary complex $Ca_x^{2+}TCa_e^{2+}$ (State 4, dead end). The intermediate complexes $T\,Ca_e^{2+}$ and $Ca_x^{2+}\,T$ are assumed not to undergo any conformational changes, as they are likely to be in negligible concentrations. The transport of Ca^{2+} via the mitochondrial Ca^{2+} uniporter is limited by the interconversion rate constants k_{in} and k_{out} which are dependent on the mitochondrial membrane potential $\Delta\Psi$.

Derivation of mitochondrial Ca^{2+} uniporter flux expression

Based on the proposed uniporter-mediated Ca^{2+} transport scheme (Fig. 1) and with the assumptions of a quasi-steady

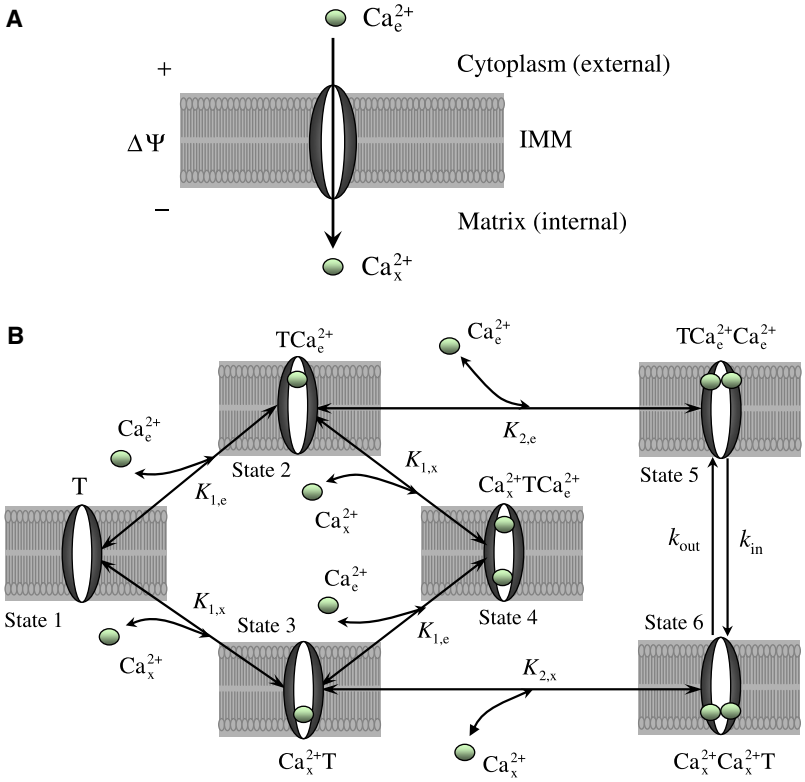

FIGURE 1 The proposed six-state kinetic mechanism of Ca^{2+} transport into mitochondria via the Ca^{2+} uniporter. The uniporter is assumed to have two binding sites for Ca^{2+} and the Ca^{2+} is assumed to bind to the uniporter from either side of the IMM. The ionized free Ca^{2+} from the cytoplasmic (*external*) side of the IMM cooperatively binds to the unbound uniporter (T) (*State 1*) in two steps to form the complex $T\,Ca_e^{2+}Ca_e^{2+}$ (*State 5*) which then undergo conformal changes (or flips upside down) to form the complex $Ca_x^{2+}Ca_x^{2+}T$ (State 6). The complex $Ca_x^{2+}Ca_x^{2+}T$ in the matrix (*internal*) side of the IMM goes through the reverse process where it dissociates in two steps to form the unbound uniporter (T) and ionized free Ca^{2+}. The model also assumes the cross-interactions between the uniporter, external Ca^{2+}, and internal Ca^{2+} to form the intermediate complex $Ca_x^{2+}TCa_e^{2+}$ (dead end, State 4). The other two states of the uniporter are the bound uniporter $T\,Ca_e^{2+}$ (*State 2*) and $Ca_x^{2+}\,T$ (*State 3*). ($K_{1,e}$, $K_{1,x}$) and ($K_{2,e}$, $K_{2,x}$) are the two pairs of dissociation (binding) constants for the two step uniporter binding reactions with the external and internal Ca^{2+}. The transport of Ca^{2+} via the Ca^{2+} uniporter is limited by the rate constants k_{in} and k_{out} which are dependent on the membrane potential $\Delta\Psi$.

state, rapid equilibrium binding of the external and internal Ca^{2+} with the uniporter, the reactions for the uniporter-Ca^{2+} binding and the reaction for the conformational change of the ternary uniporter-$2Ca^{2+}$ binding complex can be written as

$$
\begin{aligned}
&T + Ca_e^{2+} \underset{K_{1,e}}{\leftrightarrow} TCa_e^{2+}, \quad T + Ca_x^{2+} \underset{K_{1,x}}{\leftrightarrow} Ca_x^{2+}T,\\
&TCa_e^{2+} + Ca_x^{2+} \underset{K_{1,x}}{\leftrightarrow} Ca_x^{2+}TCa_e^{2+},\\
&Ca_x^{2+}T + Ca_e^{2+} \underset{K_{1,e}}{\leftrightarrow} Ca_x^{2+}TCa_e^{2+},\\
&TCa_e^{2+} + Ca_e^{2+} \underset{K_{2,e}}{\leftrightarrow} TCa_e^{2+}Ca_e^{2+},\\
&Ca_x^{2+}T + Ca_x^{2+} \underset{K_{2,x}}{\leftrightarrow} Ca_x^{2+}Ca_x^{2+}T,\\
&TCa_e^{2+}Ca_e^{2+} \underset{k_{out}}{\overset{k_{in}}{\rightleftarrows}} Ca_x^{2+}Ca_x^{2+}T,
\end{aligned}
\tag{1}
$$

where ($K_{1,e}$, $K_{1,x}$) and ($K_{2,e}$, $K_{2,x}$) are the two pairs of dissociation (binding) constants for the two step uniporter binding reactions with the external and internal Ca^{2+}; k_{in} and k_{out} are the forward and reverse rate constants in the interconversion of $T\,Ca_e^{2+}Ca_e^{2+}$ and $Ca_x^{2+}Ca_x^{2+}T$, which limit the uniporter function. Since the conformational change or interconversion of $T\,Ca_e^{2+}Ca_e^{2+}$ (State 5) into $Ca_x^{2+}Ca_x^{2+}T$ (State 6) involves translocation of positive charges (Ca^{2+}), the rate constants k_{in} and k_{out} are functions of membrane potential $\Delta\Psi$. Furthermore, depending on physical locations of the Ca^{2+} binding sites on the uniporter, the binding constants $K_{1,e}$, $K_{1,x}$, $K_{2,e}$, and $K_{2,x}$ can also be dependent on membrane potential $\Delta\Psi$.

Under the quasi-steady state, rapid equilibrium binding assumptions, we have the following relationships between various states of the uniporter:

$$
\begin{aligned}
&\left[TCa_e^{2+}\right] = \frac{\left[Ca^{2+}\right]_e}{K_{1,e}}[T], \quad \left[Ca_x^{2+}T\right] = \frac{\left[Ca^{2+}\right]}{K_{1,x}}[T],\\
&\left[TCa_e^{2+}Ca_e^{2+}\right] = \frac{\left[Ca^{2+}\right]_e^2}{K_{1,e}K_{2,e}}[T],\\
&\left[Ca_x^{2+}Ca_x^{2+}T\right] = \frac{\left[Ca^{2+}\right]_x^2}{K_{1,x}K_{2,x}}[T],\\
&\left[Ca_x^{2+}TCa_e^{2+}\right] = \frac{\left[Ca^{2+}\right]_x\left[Ca^{2+}\right]_e}{K_{1,x}K_{1,e}}[T],
\end{aligned}
\tag{2}
$$

where the concentrations of free and Ca^{2+}-bound uniporter states are expressed with respect to the mitochondrial matrix volume; $[Ca^{2+}]_e$ and $[Ca^{2+}]_x$ denote the extra-mitochondrial and matrix concentrations of Ca^{2+}; $K_{1,e}$, $K_{1,x}$, $K_{2,e}$, and $K_{2,x}$ are in the units of concentration (molar).

Since the total uniporter concentration $[T]_{tot}$ is constant, we have by mass conservation

$$
\begin{aligned}
&[T] + \left[TCa_e^{2+}\right] + \left[Ca_x^{2+}T\right] + \left[Ca_x^{2+}TCa_e^{2+}\right]\\
&\quad + \left[TCa_e^{2+}Ca_e^{2+}\right] + \left[Ca_x^{2+}Ca_x^{2+}T\right] = [T]_{tot}.
\end{aligned}
\tag{3}
$$

Upon substituting Eq. 2 into Eq. 3 and by rearranging, we can express the concentration of unbound free uniporter [T] in terms of the total uniporter concentration $[T]_{tot}$ as

$$[\mathrm{T}] = [\mathrm{T}]_{\mathrm{tot}}/D, \tag{4}$$

where

$$D = 1 + \frac{[\mathrm{Ca}^{2+}]_{\mathrm{e}}}{K_{1,\mathrm{e}}} + \frac{[\mathrm{Ca}^{2+}]_{\mathrm{x}}}{K_{1,\mathrm{x}}} + \frac{[\mathrm{Ca}^{2+}]_{\mathrm{e}}[\mathrm{Ca}^{2+}]_{\mathrm{x}}}{K_{1,\mathrm{e}}K_{1,\mathrm{x}}} + \frac{[\mathrm{Ca}^{2+}]_{\mathrm{e}}^2}{K_{1,\mathrm{e}}K_{2,\mathrm{e}}} + \frac{[\mathrm{Ca}^{2+}]_{\mathrm{x}}^2}{K_{1,\mathrm{x}}K_{2,\mathrm{x}}}. \tag{5}$$

According to the proposed scheme of Ca^{2+} transport into mitochondria via the Ca^{2+} uniporter (Fig. 1), the Ca^{2+} transport flux (due to conformational change) can be expressed as

$$J_{\mathrm{Uni}} = k_{\mathrm{in}}[\mathrm{TCa}_{\mathrm{e}}^{2+}\mathrm{Ca}_{\mathrm{e}}^{2+}] - k_{\mathrm{out}}[\mathrm{Ca}_{\mathrm{x}}^{2+}\mathrm{Ca}_{\mathrm{x}}^{2+}\mathrm{T}] = \frac{[\mathrm{T}]_{\mathrm{tot}}}{D}\left(k_{\mathrm{in}}\frac{[\mathrm{Ca}^{2+}]_{\mathrm{e}}^2}{K_{1,\mathrm{e}}K_{2,\mathrm{e}}} - k_{\mathrm{out}}\frac{[\mathrm{Ca}^{2+}]_{\mathrm{x}}^2}{K_{1,\mathrm{x}}K_{2,\mathrm{x}}}\right). \tag{6}$$

The generalized flux expression (6) contains four binding constants ($K_{1,\mathrm{e}}$, $K_{1,\mathrm{x}}$, $K_{2,\mathrm{e}}$ and $K_{2,\mathrm{x}}$) and two rate constants (k_{in} and k_{out}), that is a total of six unknown kinetic parameters. The number of kinetic parameters can be reduced by two with the following simplifications.

Model 1

In one approximation, the first binding constants $K_{1,\mathrm{e}}$ and $K_{1,\mathrm{x}}$ are assumed to be large compared to the second binding constants $K_{2,\mathrm{e}}$ and $K_{2,\mathrm{x}}$ with the constraints that $K_{1,\mathrm{e}}.K_{2,\mathrm{e}} = {K_{\mathrm{e}}}^2$ and $K_{1,\mathrm{x}}.K_{2,\mathrm{x}} = {K_{\mathrm{x}}}^2$ are finite (cooperative binding). These approximations are valid under the assumptions $K_{1,\mathrm{e}} \gg 1\ \mu\mathrm{M}$, $K_{1,\mathrm{x}} \gg 1\ \mu\mathrm{M}$, $K_{2,\mathrm{e}} \ll 1\ \mu\mathrm{M}$, and $K_{2,\mathrm{x}} \ll 1\ \mu\mathrm{M}$. In this case, the concentrations of $\mathrm{T}\,\mathrm{Ca}_{\mathrm{e}}^{2+}$, $\mathrm{Ca}_{\mathrm{x}}^{2+}\mathrm{T}$ and $\mathrm{Ca}_{\mathrm{x}}^{2+}\mathrm{T}\,\mathrm{Ca}_{\mathrm{e}}^{2+}$ can be considered negligible compared to the concentrations of the other binding states of the uniporter. The flux expression (6) reduces to

$$J_{\mathrm{Uni}} = \frac{[\mathrm{T}]_{\mathrm{tot}}}{D_1}\left(k_{\mathrm{in}}\frac{[\mathrm{Ca}^{2+}]_{\mathrm{e}}^2}{K_{\mathrm{e}}^2} - k_{\mathrm{out}}\frac{[\mathrm{Ca}^{2+}]_{\mathrm{x}}^2}{K_{\mathrm{x}}^2}\right), \tag{7}$$

where

$$D_1 = 1 + \frac{[\mathrm{Ca}^{2+}]_{\mathrm{e}}^2}{K_{\mathrm{e}}^2} + \frac{[\mathrm{Ca}^{2+}]_{\mathrm{x}}^2}{K_{\mathrm{x}}^2}. \tag{8}$$

The reduced flux expression (7) contains only two binding constants (K_{e} and K_{x}) and two rate constants (k_{in} and k_{out}), a total of four unknown kinetic parameters.

Model 2

In another approximation, the first binding constants $K_{1,\mathrm{e}}$ and $K_{1,\mathrm{x}}$ are assumed to be equal to the second binding constants $K_{2,\mathrm{e}}$ and $K_{2,\mathrm{x}}$, respectively; $K_{1,\mathrm{e}} = K_{2,\mathrm{e}} = K_{\mathrm{e}}$ and $K_{1,\mathrm{x}} = K_{2,\mathrm{x}} = K_{\mathrm{x}}$. In this case, the flux expression (6) reduces to

$$J_{\mathrm{Uni}} = \frac{[\mathrm{T}]_{\mathrm{tot}}}{D_2}\left(k_{\mathrm{in}}\frac{[\mathrm{Ca}^{2+}]_{\mathrm{e}}^2}{K_{\mathrm{e}}^2} - k_{\mathrm{out}}\frac{[\mathrm{Ca}^{2+}]_{\mathrm{x}}^2}{K_{\mathrm{x}}^2}\right), \tag{9}$$

where

$$D_2 = 1 + \frac{[\mathrm{Ca}^{2+}]_{\mathrm{e}}}{K_{\mathrm{e}}} + \frac{[\mathrm{Ca}^{2+}]_{\mathrm{x}}}{K_{\mathrm{x}}} + \frac{[\mathrm{Ca}^{2+}]_{\mathrm{e}}[\mathrm{Ca}^{2+}]_{\mathrm{x}}}{K_{\mathrm{e}}K_{\mathrm{x}}} + \frac{[\mathrm{Ca}^{2+}]_{\mathrm{e}}^2}{K_{\mathrm{e}}^2} + \frac{[\mathrm{Ca}^{2+}]_{\mathrm{x}}^2}{K_{\mathrm{x}}^2}. \tag{10}$$

As in the case of Model 1, the reduced flux expression (9) contains only two binding constants (K_{e} and K_{x}) and two rate constants (k_{in} and k_{out}), a total of four unknown kinetic parameters. However, the denominator D_2 is more complex (it contains the contributions from State 2, State 3 and State 4) than the denominator D_1. Therefore, even if both models may be able to fit to the same experimental data, the estimates of the kinetic parameters K_{e}, K_{x}, k_{in} and k_{out} from these two models are expected to differ.

Further parameter reduction

Under equilibrium transport conditions, the flux of Ca^{2+} via the Ca^{2+} uniporter is zero (i.e., $J_{\mathrm{Uni}} = 0$). Therefore, the kinetic parameters K_{e}, K_{x}, k_{in} and k_{out} can be further constrained by the following equilibrium relationships:

$$\frac{k_{\mathrm{in}}.K_{\mathrm{x}}^2}{k_{\mathrm{out}}.K_{\mathrm{e}}^2} = \frac{[\mathrm{Ca}^{2+}]_{\mathrm{x,eq}}^2}{[\mathrm{Ca}^{2+}]_{\mathrm{e,eq}}^2} = K_{\mathrm{eq}}, \tag{11}$$

where K_{eq} is the equilibrium constant for trans-membrane Ca^{2+} transport which is a function of membrane potential $\Delta\Psi$ (see below). Therefore, the number of unknown kinetic parameters for estimation can be further reduced by one (from four parameters to three parameters).

It is to be noted here that the electrostatic field of the charged membrane will influence both the stages of ternary uniporter-$2Ca^{2+}$ complex formation and the stages of trans-membrane Ca^{2+} translocation via the uniporter. We consider below the most general case of interactions between the electric field of the membrane and molecules taking part in Ca^{2+} translocation. Such interactions are described via dependencies of the kinetic parameters K_{e}, K_{x}, k_{in} and k_{out} on the electrostatic potential difference of the membrane.

Dependence of kinetic parameters K_{e}, K_{x}, k_{in} and k_{out} on membrane potential $\Delta\Psi$

The binding of Ca^{2+} to the uniporter and the translocation of Ca^{2+} via the uniporter depends on the electrostatic field of the charged membrane. To take this dependency into account, we assume that the kinetic parameters (dissociation and rate constants: K_{e}, K_{x}, k_{in} and k_{out}) depend on the electrostatic potential difference across the membrane. The membrane potential dependencies of the kinetic parameters can be derived based on biophysical principles and well-known laws of thermodynamics, electrostatics and superposition. Our approach is similar to that of Metelkin et al. (31) on the kinetic modeling of mitochondrial adenine nucleotide translocase. In this

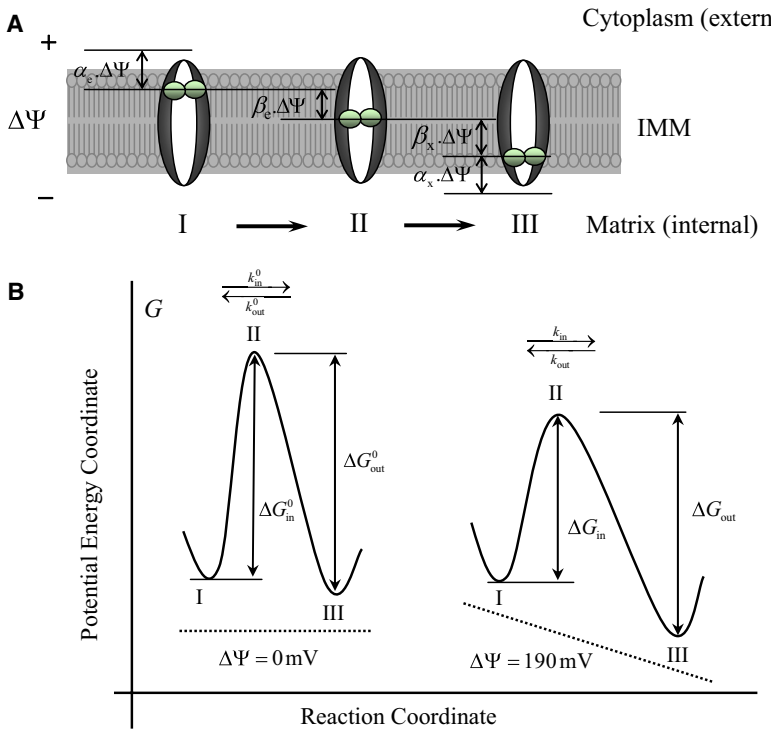

FIGURE 2 Free-energy barrier formalism for Ca^{2+} transport into mitochondria via the Ca^{2+} uniporter. (*A*) (*I–III*) Consecutive states of the Ca^{2+}-bound uniporter functional unit in the process of Ca^{2+} translocation that is used to derive the dependence of the rate of Ca^{2+} transport on the electrostatic membrane potential $\Delta\Psi$. Here, α_e is the ratio of the potential difference between Ca^{2+} bound at the site of uniporter facing the external side of the IMM and Ca^{2+} in the bulk phase to the total membrane potential $\Delta\Psi$, α_x is the ratio of the potential difference between Ca^{2+} bound at the site of uniporter facing the internal side of the IMM and Ca^{2+} in the bulk phase to the total membrane potential $\Delta\Psi$, β_e is the displacement of external Ca^{2+} from the coordinate of maximum potential barrier, and β_x is the displacement of internal Ca^{2+} from the coordinate of maximum potential barrier. (*B*) Potential energy barrier profile along the reaction coordinate that is used to derive the dependence of the rate of Ca^{2+} transport on the electrostatic membrane potential $\Delta\Psi$. The dashed line shows the profile of the potential created by the electric field of the charged membrane. The points I, II, and III correspond to the Ca^{2+}-bound uniporter states depicted in the upper panel *A*. The rate constants k_{in} and k_{out} are related to the changes in potential energy (Gibbs free-energy) ΔG_{in} and ΔG_{out}. Note that in the absence of electric field ($\Delta\Psi = 0$ mV), the heights of the free-energy barriers in the forward and reverse directions are equal when the dissociation constants for the binding of the external and internal Ca^{2+} to the uniporter are equal: that is, $\Delta G_{in}^0 = \Delta G_{out}^0 = \Delta G^0$ if and only if $K_e^0 = K_x^0 = K^0$.

approach, we assume that the total value of the membrane potential is the sum of local electric potentials and each of the local electric potentials influences the corresponding stages of the Ca^{2+} binding and translocation processes.

The stages of Ca^{2+} binding to the uniporter and Ca^{2+} translocation via the uniporter are schematized in Fig. 2. Every position of Ca^{2+} on the uniporter can be characterized by an electric potential value. We assume here that the difference in potentials between the adjacent positions of Ca^{2+} is proportional to the total potential difference across the membrane. In accordance with the rule of superposition, the sum of potential differences between the consecutive positions of Ca^{2+} is equal to the total potential difference across the membrane. Thus, this approach divides the total drop in potential across the membrane into elementary stages. The scheme depicted in Fig. 2 illustrates the influence of such elementary potential drops on the rate of uniporter operation. Values of the potential drops are marked for all elementary stages of the scheme.

Equilibrium constant

Since a cycle of uniporter operation involves translocation of four elementary positive charges ($2Ca^{2+}$) across the mitochondrial membrane, the dependence of the equilibrium constant K_{eq} on the membrane potential $\Delta\Psi$ for the uniporter-mediated Ca^{2+} transport across the membrane can be expressed as (Nernst equation)

$$K_{eq} = \exp(2\Delta\Phi),\ \Delta\Phi = Z_{Ca}F\Delta\Psi/RT, \qquad (12)$$

where $Z_{Ca} = 2$ is the valence of Ca^{2+}; F, R, and T denote the Faraday's constant, ideal gas constant, and absolute temperature, respectively; $\Delta\Phi$ is the nondimensional potential difference across the membrane. In the absence of electric field ($\Delta\Psi = 0$), Eq. 12 gives $K_{eq} = 1$.

Dissociation constants

To derive the dependence of the dissociation constants of uniporter-Ca^{2+} binding on the membrane potential $\Delta\Psi$, let us first consider the two-step binding of the external Ca^{2+} to the uniporter. The changes in Gibb's free-energy for the two binding reactions are

$$\begin{aligned}\Delta\mu_{1,e} &= \Delta\mu_{1,e}^0 + Z_{Ca}F\alpha_e\Delta\Psi \\ &\quad + RT\ln\left([T]\left[Ca^{2+}\right]_e/\left[TCa_e^{2+}\right]\right), \\ \Delta\mu_{2,e} &= \Delta\mu_{2,e}^0 + Z_{Ca}F\alpha_e\Delta\Psi \\ &\quad + RT\ln\left(\left[TCa_e^{2+}\right]\left[Ca^{2+}\right]_e/\left[TCa_e^{2+}Ca_e^{2+}\right]\right),\end{aligned} \qquad (13)$$

where $\Delta\mu_{1,e}^0$ and $\Delta\mu_{2,e}^0$ are the standard changes in Gibbs free-energy of the reactions; α_e is the ratio of the potential difference between Ca^{2+} bound at the site of uniporter facing the external side of the IMM and Ca^{2+} in the bulk phase to the total membrane potential $\Delta\Psi$ ($\Delta\Psi = \Psi_e - \Psi_x$, i.e., outside potential minus inside potential, so $\Delta\Psi$ is positive). An assumption inherent in this derivation is that both the Ca^{2+} binding sites on the uniporter are at an equidistant distance from the bulk medium. At equilibrium ($\Delta\mu_{1,e} = \Delta\mu_{2,e} = 0$), Eq. 13 gives

$$\begin{aligned} K_{1,e} &= \left([\mathrm{T}]\left[\mathrm{Ca}^{2+}\right]_e/[\mathrm{TCa}_e^{2+}]\right)_{eq} \\ &= K_{1,e}^0 \exp(-\alpha_e \Delta\Phi), \\ K_{2,e} &= \left(\left[\mathrm{TCa}_e^{2+}\right]\left[\mathrm{Ca}^{2+}\right]_e/[\mathrm{TCa}_e^{2+}\mathrm{Ca}_e^{2+}]\right)_{eq} \\ &= K_{2,e}^0 \exp(-\alpha_e \Delta\Phi), \end{aligned} \tag{14}$$

where $K_{1,e}^0 = K_{1,e}(\Delta\Psi = 0) = \exp(-\Delta\mu_{1,e}^0/RT)$ and $K_{2,e}^0 = K_{2,e}(\Delta\Psi = 0) = \exp(-\Delta\mu_{2,e}^0/RT)$. Equation 14 suggests that the dissociation constants $K_{1,e}$ and $K_{2,e}$ for binding of the external Ca^{2+} to the uniporter are reduced (i.e., the association becomes easier) in the presence of electric field, provided $\alpha_e > 0$.

For binding of the internal Ca^{2+} to the uniporter, it can be similarly shown that

$$\begin{aligned} K_{1,x} &= \left([\mathrm{T}]\left[\mathrm{Ca}^{2+}\right]_x/[\mathrm{Ca}_x^{2+}\mathrm{T}]\right)_{eq} \\ &= K_{1,x}^0 \exp(+\alpha_x \Delta\Phi), \\ K_{2,x} &= \left(\left[\mathrm{Ca}_x^{2+}\mathrm{T}\right]\left[\mathrm{Ca}^{2+}\right]_x/[\mathrm{Ca}_x^{2+}\mathrm{Ca}_x^{2+}\mathrm{T}]\right)_{eq} \\ &= K_{2,x}^0 \exp(+\alpha_x \Delta\Phi), \end{aligned} \tag{15}$$

where α_x is the ratio of the potential difference between Ca^{2+} bound at the site of uniporter facing the internal side of the IMM and Ca^{2+} in the bulk phase to the total membrane potential $\Delta\Psi$. In contrast to $K_{1,e}$ and $K_{2,e}$, the dissociation constants $K_{1,x}$ and $K_{2,x}$ for binding of the internal Ca^{2+} to the uniporter are increased (i.e., the association becomes difficult) in the presence of electric field, provided $\alpha_x > 0$.

In either of the models derived in the previous section (Model 1 and Model 2), the dissociation constants K_e and K_x can be obtained from Eqs. 14 and 15 as

$$K_e = K_e^0 \exp(-\alpha_e \Delta\Phi) \quad \text{and} \quad K_x = K_x^0 \exp(+\alpha_x \Delta\Phi). \tag{16}$$

Note that for more generality we have assumed here that K_e^0 and K_x^0 are distinct. Thus the dissociation constants K_e and K_x can be fully characterized by four unknown parameters K_e^0, K_x^0, α_e and α_x. For positive α_e and α_x, the dissociation constant tends to decrease on the outside and increase on the inside of the IMM.

Rate constants

The influence of the membrane potential $\Delta\Psi$ on the rate constants of the ternary uniporter-$2Ca^{2+}$ complex conformational change can be accounted for using Eyring's free-energy barrier theory for absolute reaction rates and electrodiffusion (25–28). For simplicity, we assume here that the free-energy profile of Ca^{2+} translocation across the membrane (limiting stage) is a single barrier (Fig. 2 *B*), and the translocation is a jump over the barrier from one potential well to another. We define the reaction coordinate as the coordinate from Ca^{2+} bound at the external side to Ca^{2+} bound at the internal side of the membrane along the direction of Ca^{2+} translocation. The local maximum (peak) (State II) of the free-energy profile corresponds to the barrier that impedes the Ca^{2+} translocation, whereas the local minima (States I and III) correspond to the uniporter-$2Ca^{2+}$ complex states on the either side of the membrane. The Ca^{2+} transport rate is determined by the probability of the uniporter to translocate Ca^{2+} from one binding site to the other, which depends on the height of the free-energy barrier, which in turn depends on the membrane potential $\Delta\Psi$, as schematized in Fig. 2 *B*.

According to Eyring's free-energy barrier theory, the rate at which an ion can jump from one binding site to the other is given by

$$k = \kappa \exp(-\Delta G/RT), \tag{17}$$

where ΔG is the height of the free-energy barrier; $\kappa = k_B T/h$ is a constant (with units of 1/time), where k_B is Boltzmann's constant, h is Planck's constant, and T is the temperature. In this case, the heights of the free-energy barrier (State II) from States I and III can be defined by

$$\begin{aligned} \Delta G_{in} &= \Delta G_{in}^0 - 2Z_{Ca} F \beta_e \Delta\Psi, \\ \Delta G_{out} &= \Delta G_{out}^0 + 2Z_{Ca} F \beta_x \Delta\Psi, \end{aligned}$$

where ΔG_{in}^0 and ΔG_{out}^0 are the heights of the free-energy barriers in the absence of electric field ($\Delta\Psi = 0$ mV), β_e is the displacement of external Ca^{2+} (State I) from the coordinate of maximum potential barrier (State II), and β_x is the displacement of internal Ca^{2+} (State III) from the coordinate of maximum potential barrier (State II). Note that $\Delta G_{in}^0 = \Delta G_{out}^0 = \Delta G^0$ subject to the condition $K_e^0 = K_x^0 = K^0$. For simplicity, we have assumed that the uniporter has no net charge (neutral) and that the charge on the uniporter-$2Ca^{2+}$ complex is $2Z_{Ca}$. Otherwise, we could express $\beta_e = (\beta_{e,Ca} + \sum Z_j \beta_{e,j}/2Z_{Ca})$ and $\beta_x = (\beta_{x,Ca} + \sum Z_j \beta_{x,j}/2Z_{Ca})$ as the effective displacement parameters that can be identified, where Z_j is the jth charged species of the uniporter and $\beta_{e,j}$ and $\beta_{x,j}$ are the corresponding displacements ($\beta_{e,Ca}$ and $\beta_{x,Ca}$ are the displacements of Ca^{2+} ions).

It is evident from Eq. 18, that the height of the barrier in the inward direction is reduced, while the height in the outward direction is increased in the presence of electric field (Fig. 2 *B*). This means it becomes easier for the Ca^{2+} ions to cross the barrier in the inward direction, but more difficult for the Ca^{2+} ions to exit the matrix in the presence of a positive membrane potential, measured from outside to inside. Upon substituting Eq. 18 into Eq. 17, we obtain the rate constants of Ca^{2+} translocation as

$$k_{in} = k_{in}^0 \exp(+2\beta_e \Delta\Phi), \; k_{out} = k_{out}^0 \exp(-2\beta_x \Delta\Phi), \tag{19}$$

where $k_{in}^0 = \kappa \exp(-\Delta G_{in}^0/RT)$ and $k_{out}^0 = \kappa \exp(-\Delta G_{out}^0/RT)$ are the forward and reverse rate constants in the absence of electric filed ($\Delta\Psi = 0$ mV). Thus the rate constants k_{in} and k_{out} can be fully characterized by four unknown parameters k_{in}^0, k_{out}^0, β_e and β_x. Also note that $k_{in}^0 = k_{out}^0 = k^0$, subject to the condition $\Delta G_{in}^0 = \Delta G_{out}^0 = \Delta G^0$ or $K_e^0 = K_x^0 = K^0$.

Thermodynamics constraint and parameter reduction

By substituting Eq. 12 for K_{eq}, Eq. 16 for K_e and K_x, and Eq. 19 for k_{in} and k_{out} into Eq. 11, we obtain the following relationships (thermodynamic constraints) between k^0_{in}, k^0_{out}, K^0_x and K^0_e and α_e, α_x, β_e and β_x:

$$\begin{aligned} \left(k^0_{in}/k^0_{out}\right).\left(K^0_x/K^0_e\right)^2 &= 1 \quad \text{and} \\ \alpha_e + \alpha_x + \beta_e + \beta_x &= 1. \end{aligned} \tag{20}$$

These thermodynamic constraints reduce the number of unknown parameters by two, from a total of eight parameters to six parameters.

Derived models of mitochondrial Ca^{2+} uniporter

By substituting Eq. 16 for K_e and K_x and Eq. 19 for k_{in} and k_{out} into Eqs. 7 and 8, and using the above thermodynamic constraint (Eq. 20), the flux expression for the mitochondrial Ca^{2+} uniporter corresponding to Model 1 (Eqs. 7 and 8) is reduced to

$$J_{Uni} = X_{Uni}\frac{\left(\left[Ca^{2+}\right]^2_e\exp(+\Delta\Phi) - \left[Ca^{2+}\right]^2_x\exp(-\Delta\Phi)\right)\exp((2\alpha_e + 2\beta_e - 1)\Delta\Phi)}{\left(K^{0\,2}_x + \left(K^0_x/K^0_e\right)^2\left[Ca^{2+}\right]^2_e\exp(2\alpha_e\Delta\Phi) + \left[Ca^{2+}\right]^2_x\exp(-2\alpha_x\Delta\Phi)\right)}, \tag{21}$$

where $X_{Uni} = [T]_{tot}.k^0_{out}$ is a lumped parameter denoting the activity of the uniporter. Note that for $\alpha_e = \alpha_x = 0$ and $K^0_e = K^0_x = K^0$, the flux expression (21) can approximate the flux expression (see Eq. S1 in the Supporting Material) in our previous model of the uniporter (15) provided $\exp((2\beta_e - 1)\Delta\Phi) \approx ((\Delta\Phi/n_{Uni})/\sinh(\Delta\Phi/n_{Uni}))^{n_{Uni}}$.

In a similar fashion, we can rewrite the flux expression for the mitochondrial Ca^{2+} uniporter corresponding to Model 2 (Eqs. 9 and 10) in the form

$$J_{Uni} = X_{Uni}\frac{\left(\left[Ca^{2+}\right]^2_e\exp(+\Delta\Phi) - \left[Ca^{2+}\right]^2_x\exp(-\Delta\Phi)\right)\exp((2\alpha_e + 2\beta_e - 1)\Delta\Phi)}{\left(\begin{array}{l} K^{0\,2}_x + \left(K^{0\,2}_x/K^0_e\right)\left[Ca^{2+}\right]_e\exp(\alpha_e\Delta\Phi) + K^0_x\left[Ca^{2+}\right]_x\exp(-\alpha_x\Delta\Phi) \\ + \left(K^0_x/K^0_e\right)\left[Ca^{2+}\right]_e\left[Ca^{2+}\right]_x\exp((\alpha_e - \alpha_x)\Delta\Phi) \\ + \left(K^0_x/K^0_e\right)^2\left[Ca^{2+}\right]^2_e\exp(2\alpha_e\Delta\Phi) + \left[Ca^{2+}\right]^2_x\exp(-2\alpha_x\Delta\Phi) \end{array}\right)}. \tag{22}$$

Both the models of the Ca^{2+} uniporter are characterized by six unknown parameters (X_{Uni}, K^0_e, K^0_x, β_e, α_e and α_x) which are estimated below based on the experimental data of Scarpa and co-workers (10,11) and Gunter and co-workers (6,18) on Ca^{2+} fluxes through the uniporter in energized mitochondria purified from rat heart and rat liver measured under varying experimental conditions (varying extra-matrix $[Ca^{2+}]$ and varying membrane potential $\Delta\Psi$).

Since in most of the experiments the matrix concentration of Ca^{2+} ($[Ca^{2+}]_x$) is low compared to the extra-matrix concentration of Ca^{2+} ($[Ca^{2+}]_e$), we may not be able to estimate (identify) all of the above six independent kinetic parameters uniquely and accurately. We explore the parameter estimation (identification) process for two feasible cases: (Case 1) $K^0_e = K^0_x$ so that $\Delta G^0_{in} = \Delta G^0_{out}$ and $k^0_{in} = k^0_{out}$, and (Case 2) K^0_e and K^0_x are distinct so that ΔG^0_{in} and ΔG^0_{out} as well as k^0_{in} and k^0_{out} are distinct. For simplicity, we also assume that $\alpha_e = 0$, that is, the Ca^{2+} binding sites on the external side of the uniporter are situated at a negligible distance from the bulk phase, so that the potential barrier the external Ca^{2+} ions would have to overcome to bind to the uniporter would be negligible. With these assumptions and approximations, the number of unknown parameters for estimation is further reduced to four in Case 1 and reduced to five in Case 2.

Statistical method of optimization and parameter estimation

The mitochondrial Ca^{2+} uniporter model parameters $\theta = (X_{Uni}, K^0_e, K^0_x, \beta_e, \alpha_e, \alpha_x)$ characterizing the experimental data of Scarpa and co-workers (10,11) and Gunter and co-workers (6,18) on mitochondrial Ca^{2+} uptake were estimated by simultaneous least-squares fitting of the model simulated outputs to the experimental data

$$\min_{\theta} E(\theta),\ E(\theta) = \sum_i^{N_{exp}}\sum_j^{N_{data}}\left(\frac{J^{data}_{Uni,j} - J^{model}_{Uni,j}(\theta)}{N_{data} \times \max(J^{data}_{Uni,j})}\right)^2 \tag{23}$$

where N_{exp} is the number of experiments and N_{data} is the number of data points in a particular experiment, $J^{data}_{Uni,j}$ are

the experimental data on Ca^{2+} influx rates via the uniporter and $J^{model}_{Uni,j}(\theta)$ are the corresponding model simulated outputs which depend on the model parameter θ, $\max(J^{data}_{Uni,j})$ is the maximum value of $J^{data}_{Uni,j}$ that is used to normalize the experimental data and model outputs. The minimization of the mean residual error (objective function) $E(\theta)$ for optimal estimation of the uniporter model parameters $\theta = (X_{Uni}, K^0_e, K^0_x, \beta_e, \alpha_e, \alpha_x)$ is carried out using the FMINCON optimizer in Matlab (The MathWorks, Natick, MA) The robustness of the model fitting to the data for a particular uniporter model is assessed based on the value of mean residual error $E(\theta)$ in Eq. 23 at the optimal parameter estimates (least-square error).

RESULTS

This section demonstrates the parameterization and independent validation of the two developed mathematical models of the mitochondrial Ca^{2+} uniporter. Specifically, the two different kinetic models of the uniporter (Model 1 and Model 2; Eqs. 21 and 22) under two different assumptions (Case 1: $K^0_e = K^0_x$ and Case 2: K^0_e and K^0_x are distinct) are used here to simulate and fit the independent experimental data of Scarpa and co-workers (10,11) and Gunter and co-workers (6,18) on mitochondrial Ca^{2+} uptake, which are shown in Figs. 3 and 4. The solid lines are the simulations from Model 1, whereas the dashed lines are the simulations from Model 2. The left

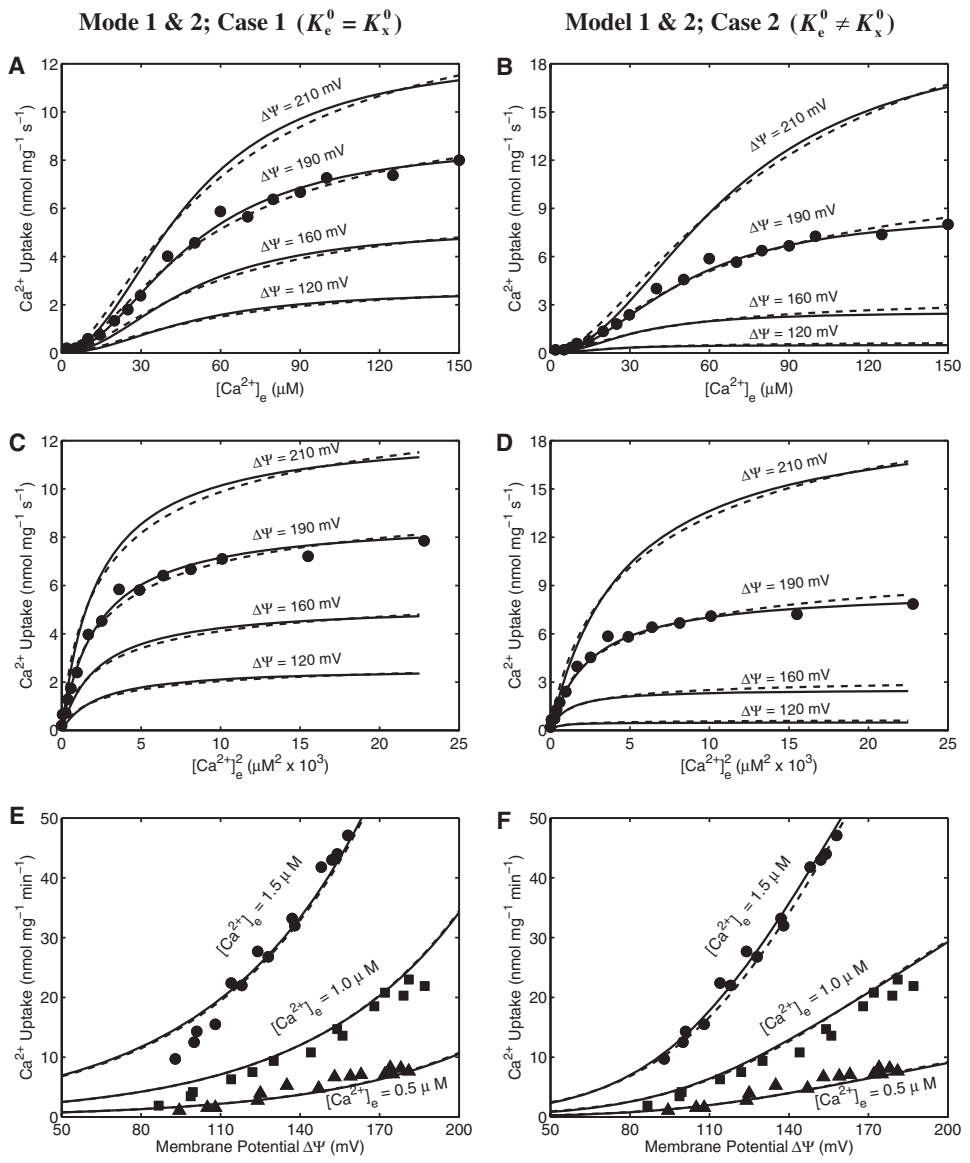

FIGURE 3 The fittings of Ca^{2+} uniporter model (*lines*) to the experimental data (points) on Ca^{2+} uptake in purified rat liver mitochondria for two different models under two different assumptions. (*Upper and middle panels*: *A–D*) The fittings of four different kinetic models of Ca^{2+} uniporter to the kinetic data of Vinogradov and Scarpa (11) in which the initial rates of Ca^{2+} uptake (*points*) were measured in respiring mitochondria purified from rat liver with varying levels of extra-matrix buffer Ca^{2+}. Also shown are the Model simulated mitochondrial Ca^{2+} uptake at four different levels of membrane potential $\Delta\Psi$ (*lines*) in which the models were fitted to the data with $\Delta\Psi = 190$ mV (States 2 and 4 membrane potential). The plots in the upper panels (*A* and *B*) differ from the plots in the middle panels (*C* and *D*) through the labeling of the *x* axis. (*Lower panels*: *E* and *F*) The fittings of the same four kinetic models to the kinetic data of Gunter and co-workers (6,18) in which the initial rates of Ca^{2+} uptake in respiring mitochondria purified from rat liver were measured with varying membrane potential $\Delta\Psi$ for three different levels of extra-matrix buffer Ca^{2+}. To fit the models to these additional data sets, only the uniporter activity parameter (X_{Uni}) is readjusted, while keeping the other kinetic parameter fixed at values as estimated from the fittings in plots (*A–D*) (Table 1). The solid lines are the simulations from Model 1 ($K_{1,e} \gg 1$, $K_{1,x} \gg 1$, $K_{2,e} \ll 1$ and $K_{2,x} \ll 1$, such that $K_{1,e}.K_{2,e} = K_e^2$ and $K_{1,x}.K_{2,x} = K_x^2$ are finite), whereas the dashed lines are the simulations from Model 2 ($K_{1,e} = K_{2,e} = K_e$ and $K_{1,x} = K_{2,x} = K_x$); the left panels (*A, C, E*) correspond to the fittings and simulations with the assumption that $K^0_e = K^0_x = K^0$, whereas the right panels (*B, D, F*) correspond to the fittings and simulations with the assumption that K^0_e and K^0_x are distinct.

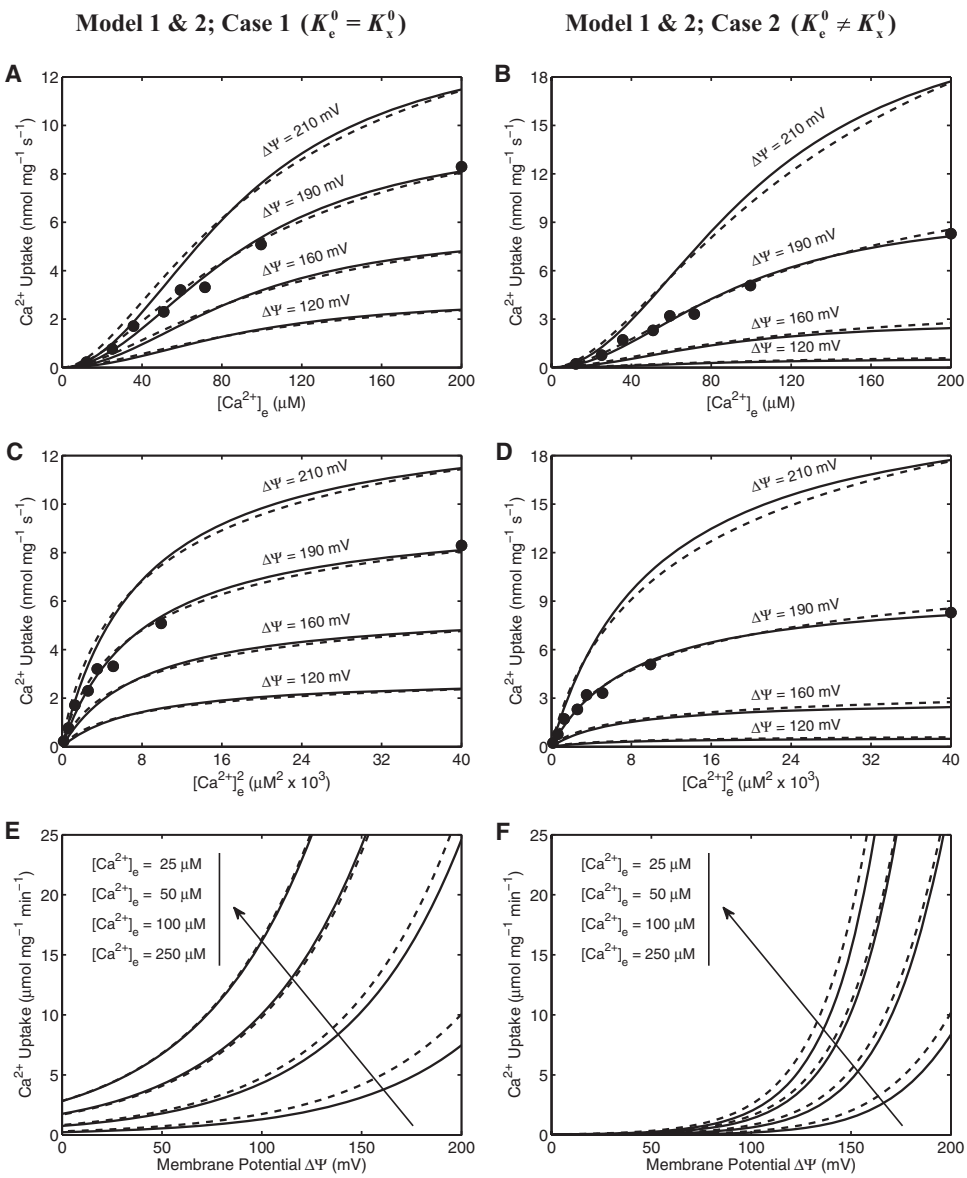

FIGURE 4 The fittings of Ca^{2+} uniporter model (lines) to the experimental data (*points*) on Ca^{2+} uptake in isolated rat heart mitochondria for two different models under two different assumptions. (*Upper and middle panels*: *A–D*) The fittings of four different kinetic models of Ca^{2+} uniporter to the kinetic data of Scarpa and Graziotti (10) in which the initial rates of Ca^{2+} uptake (*points*) were measured in respiring mitochondria isolated from rat heart with varying levels of extra-mitochondrial buffer Ca^{2+}. Also shown are the Model simulated mitochondrial Ca^{2+} uptake at four different levels of membrane potential $\Delta\Psi$ (*lines*) in which the models were fitted to the data with $\Delta\Psi = 190$ mV (States 2 and 4 membrane potential). The plots in the upper panels (*A* and *B*) differ from the plots in the middle panels (*C* and *D*) through the labeling of the *x* axis. To fit the models to these additional data sets from rat heart mitochondria, only the kinetic parameters X_{Uni}, K_e^0 and K_x^0 were readjusted, while keeping the other kinetic parameter α_e, α_x, β_e and β_x fixed at values as estimated from the fittings in Fig. 3 for rat liver mitochondria (Table 1). (*Lower panels*: *E* and *F*) The Model simulated Ca^{2+} uptake in respiring mitochondria isolated from rat heart as a function of membrane potential $\Delta\Psi$ for four different levels of extra-mitochondrial buffer Ca^{2+} (relatively higher levels of buffer Ca^{2+} than those shown in Fig. 3 *E* and *F*) for rat liver mitochondria; corresponding to the experimental protocol of Kirichok et al. (23)). For these simulations, the uniporter activity parameter (X_{Uni}) is increased by 150 times (comparable to that obtained from the data in Fig. 3 *E* and *F* for rat liver mitochondria), while keeping the other kinetic parameters fixed at values as estimated from the fittings in plots (*A–D*) (Table 1). The solid lines are the simulations from Model 1, whereas the dashed lines are the simulations from Model 2; the left panels (*A, C, E*) correspond to the fittings and simulations with the assumption that $K_e^0 = K_x^0 = K^0$, whereas the right panels (*B, D, F*) correspond to the fittings and simulations with the assumption that K_e^0 and K_x^0 are distinct; model specifications are as mentioned in Fig. 3.

panels (*A*, *C*, and *E*) of Figs. 3 and 4 correspond to the simulations and fittings for the Case 1, whereas the right panels (*B, D,* and *F*) of Figs. 3 and 4 correspond to the simulations and fittings for the Case 2. The estimated model parameter values corresponding to these different assumptions and data sets are summarized in Table 1.

In the experiments of Scarpa and co-workers, the initial (pseudo-steady) rates of Ca^{2+} uptake through the Ca^{2+} uniporter were measured in respiring mitochondria purified from rat liver (11) (Fig. 3, *A–D*) and rat heart (10) (Fig. 4, *A–D*) after the addition of varying concentrations of Ca^{2+} (i.e., $CaCl_2$) to the extra-mitochondrial buffer medium in the presence of certain amount of Mg^{2+} (i.e., $MgCl_2$). For fitting the models to the data, the membrane potential $\Delta\Psi$ is held fixed at $\Delta\Psi = 190$ mV, a typical value corresponding to the States 2 and 4 respiration. In the experiments of Gunter and co-workers, the initial (pseudo-steady) rates of Ca^{2+} uptake via the Ca^{2+} uniporter were measured in energized mitochondria isolated from rat liver as a function of membrane potential $\Delta\Psi$ for three different levels of extra-mitochondrial buffer Ca^{2+} (i.e., $[Ca^{2+}]_e = 0.5$, 1.0 and 1.5 μM) in the absence of Mg^{2+}, where the membrane potential $\Delta\Psi$ was varied through addition of varying levels of malonate to the buffer medium (6,18) (Fig. 3, *E* and *F*). These experiments provide sufficient sensitive data on the membrane potential-dependent mitochondrial Ca^{2+} uptake

TABLE 1 The estimated parameter values in the models of mitochondrial Ca^{2+} uniporter

Parameter	Values for Model 1		Values for Model 2		Units	Reference
	Case 1 ($K_e^0 = K_x^0$)	Case 2 ($K_e^0 \neq K_x^0$)	Case 1 ($K_e^0 = K_x^0$)	Case 2 ($K_e^0 \neq K_x^0$)		
k_{in}^0	49.6	0.55	36.0	0.5	nmol/mg/sec	a
	0.32	3.55×10^{-3}	0.40	5.56×10^{-3}		b
	0.354	3.986×10^{-3}	0.45	6.76×10^{-3}		c
k_{out}^0	49.6	8.5×10^{-3}	36.0	0.028	nmol/mg/sec	a
	0.32	54.84×10^{-6}	0.40	311.1×10^{-6}		b
	0.354	61.59×10^{-6}	0.45	378.4×10^{-6}		c
K_e^0	48×10^{-6}	15×10^{-6}	40×10^{-6}	12×10^{-6}	molar	a
	48×10^{-6}	15×10^{-6}	40×10^{-6}	12×10^{-6}		b
	90×10^{-6}	78.75×10^{-6}	75×10^{-6}	63×10^{-6}		c
K_x^0	48×10^{-6}	1.865×10^{-6}	40×10^{-6}	2.84×10^{-6}	molar	a
	48×10^{-6}	1.865×10^{-6}	40×10^{-6}	2.84×10^{-6}		b
	90×10^{-6}	9.79×10^{-6}	75×10^{-6}	14.91×10^{-6}		c
α_e	0	0	0	0	unitless	a, b, c
α_x	0.038	−0.214	0.038	−0.239	unitless	a, b, c
β_e	0.112	0.264	0.112	0.259	unitless	a, b, c
β_x	0.85	0.95	0.85	0.98	unitless	a, b, c
Standard physiochemical/thermodynamic parameters used in the model						
RT	Gas constant times temperature (298 K)			2.5775	kJ mol^{-1}	d
F	Faraday's constant			0.096484	kJ mol^{-1} mV^{-1}	d
Z_{Ca}	Valence of Ca^{2+}			2	unitless	d

The rate constants k_{in}^0 and k_{out}^0 are redefined here as $k_{in}^0 = [T]_{tot}.k_{in}^0$ and $k_{out}^0 = [T]_{tot}.k_{out}^0$. The uniporter activity parameter X_{Uni} in Eqs. 21 and 22 is $k_{out}^0 = [T]_{tot}.k_{out}^0$. The kinetic and biophysical parameters satisfy the thermodynamic constraints: $(k_{in}^0/k_{out}^0).(K_x^0/K_e^0)^2 = 1$ and $\alpha_e + \alpha_x + \beta_e + \beta_x = 1$. The rate constants and the uniporter activity parameters in the units of mmol/mg/s can be converted to the units of mmol/L/s by using the conversion factor 1 mg mitochondrial protein = 3.67 μL mitochondria (15).a, Estimated from the data of Wingrove et al. (18) using rat liver mitochondria; b, estimated from the data of Vinogradov & Scarpa (11) using rat liver mitochondria; c, estimated from the data of Scarpa & Graziotti (10) using rat heart mitochondria; and d, standard physiochemical/thermodynamic parameters.

at lower concentrations of extra-mitochondrial buffer Ca^{2+} for effective identification of membrane potential-dependent biophysical parameters of the model. The corresponding model simulations of the membrane potential-dependent Ca^{2+} uptake via the Ca^{2+} uniporter in respiring cardiac mitochondria with comparable uniporter activity as obtained from the data in Fig. 3, *E* and *F* for liver mitochondria but higher levels of extra-mitochondrial buffer Ca^{2+} (i.e., $[Ca^{2+}]_e$ = 25, 50, 100 and 250 μM) are shown in Fig. 4, *E* and *F* in which the membrane potential $\Delta\Psi$ was ramped from 0 mV to 200 mV—a simulation protocol similar to the experimental protocol of Kirichok et al. (23) in which the Ca^{2+} currents through the Ca^{2+} uniporter were measured using patch-clamp techniques in mitoplasts obtained from cardiac mitochondria.

From our model simulations and fittings of the models to the experimental data (Figs. 3 and 4), it is evident that both the kinetic models of the mitochondrial Ca^{2+} uniporter (Model 1 and Model 2; *solid lines* and *dashed lines*) are indistinguishable. With either of the models, we are able to reproduce the experimental data with almost identical accuracy, with suitable changes in the model parameter values, in consistent with the model assumptions. The model parameter values are different depending on the model used (Model 1 versus Model 2) or the assumptions considered (Case 1 versus Case 2) for model simulations of the experimental data (Table 1). However, it is clear from Figs. 3 and 4 that the assumptions of Case 1 and Case 2 predict significantly different behavior of mitochondrial Ca^{2+} uptake.

Both the kinetic models of the mitochondrial Ca^{2+} uniporter under both the assumptions (Case 1: $K_e^0 = K_x^0$ and Case 2: K_e^0 and K_x^0 are distinct) are able to satisfactorily describe the two independent data sets of Scarpa and co-workers on extra-mitochondrial Ca^{2+}-dependent Ca^{2+} uptake in isolated rat liver (11) and rat heart (10) mitochondria, as shown in Fig. 3, *A–D* and Fig. 4, *A–D*. However, the models with the assumption of $K_e^0 = K_x^0$ (Case 1) are not able to simulate the data sets of Gunter and co-workers on membrane potential $\Delta\Psi$-dependent Ca^{2+} uptake in purified rat liver mitochondria (6,18) (Fig. 3 *E*), especially in the domain $\Delta\Psi \leq 120$ mV. In this domain, the membrane potential factor $X_{Uni}\exp[(2\beta_e - 1)\Delta\Phi]$ in the model (Eq. 21) deviates from the empirical factor $X_{Uni}\,[(\Delta\Phi/n_{Uni})/\sinh(\Delta\Phi/n_{Uni})]^{n_{Uni}}$ in our previous model of the uniporter (15) (Eq. S1 and Fig. S1). Only the models with the assumption that K_e^0 and K_x^0 are distinct (Case 2) are able to fit to these observed kinetic data (Fig. 3 *F*). This analysis suggests that both kinds of kinetic data are essential to uniquely identify the model and the kinetic and biophysical parameters associated with the model. It is also to be noted here that either of

the kinetic models (Model 1 or Model 2) with the condition that K_e^0 and K_x^0 are distinct fit all of the available kinetic data sets (Figs. 3 and 4, *right panels*) significantly better than the kinetic models of Magnus and Keizer (16) and Jafri and co-workers (21,22) (Eqs. S2 and S3 and Figs. S2 and S3).

From this analysis, it is apparent that the extra-mitochondrial Ca^{2+}-dependent mitochondrial Ca^{2+} uptake data are essential to identify the binding constants (K_e^0 and K_x^0) of the model, whereas the membrane potential $\Delta\Psi$-dependent Ca^{2+} uptake data are necessary to identify the asymmetry of the external and internal binding constants (i.e., the notion that K_e^0 and K_x^0 are distinct) and the other biophysical parameters α_e, α_x, β_e and β_x of the model that govern the dependence of the binding constants (K_e and K_x) and rate constants (k_{in} and k_{out}) on the membrane potential $\Delta\Psi$. Therefore, the kinetic and biophysical parameters of the models were estimated by simultaneously fitting the models to both kinds of kinetic data sets from a single mitochondrial source (i.e., the Ca^{2+} uptake data from rat liver mitochondria; Fig. 3). This approach enabled robust (unique and accurate) estimations for the model parameters. Since both the data sets were from the rat liver mitochondria, the binding constants (K_e^0 and K_x^0) were constrained to be the same for both the data sets, whereas the activity parameters (k_{in}^0 and k_{out}^0) were assumed to vary over the data sets to implicitly account for different experimental protocols used in the studies of Vinogradov and Scarpa (11) and Wingrove et al. (18) (i.e., the presence versus the absence of Mg^{2+} in the extra-mitochondrial buffer medium). For Ca^{2+} uptake data of Scarpa and Graziotti (10) from the rat heart mitochondria, the binding constants (K_e^0 and K_x^0) and the activity parameters (k_{in}^0 and k_{out}^0) were allowed to be different from that obtained for the rat liver mitochondria. The biophysical parameters α_e, α_x, β_e and β_x were constrained to be the same for all three data sets, which is depicted in the estimated parameter values summarized in Table 1; the estimated values of α_e, α_x, β_e and β_x are the same for all three data sets for a particular model (Model 1 or Model 2) under a particular assumption (Case 1 or Case 2).

The fitting of the Model 1 under Case 2 to the kinetic data from cardiac mitochondria (10) (Fig. 4, *B* and *D*, *solid lines*) provides the estimates $K_e^0 = 78.75\ \mu M$, $K_x^0 = 9.8\ \mu M$, $k_{in}^0 = 4\times10^{-3}$ nmol/mg/s, and $k_{out}^0 = 61.6\times10^{-6}$ nmol/mg/s, whereas the same fitting for liver mitochondria (11) (Fig. 3, *B* and *D*, *solid lines*) provides the estimates $K_e^0 = 15\ \mu M$, $K_x^0 = 1.9\ \mu M$, $k_{in}^0 = 3.55\times10^{-3}$ nmol/mg/s, and $k_{out}^0 = 54.8\times10^{-6}$ nmol/mg/s. Thus the uniporter activities are similar in both liver and cardiac mitochondria under similar experimental conditions (both in the presence of Mg^{2+} in the experimental buffer medium), whereas the binding constants of Ca^{2+} for the uniporter in cardiac mitochondria are estimated to be ~5.25 times that of the values in liver mitochondria. The simultaneous fitting of the same kinetic model of the uniporter (Model 1, Case 2) to the other three data sets from liver mitochondria (6,18) (Fig. 3 *F*, *solid lines*) provides the similar estimates for the binding constant ($K_e^0 = 15\ \mu M$ and $K_x^0 = 1.9\ \mu M$), but about two-order of magnitude higher (~155 times) in the estimates of the uniporter activity parameters ($k_{in}^0 = 0.55$ nmol/mg/s and $k_{out}^0 = 8.5\times10^{-3}$ nmol/mg/s) than that obtained from the fitting in Fig. 3, *B* and *D* (11). The differences may be attributed to the fact that the data were from two different mitochondrial preparations and two different experimental protocols (e.g., in the presence versus absence of Mg^{2+} in the two experimental buffer mediums, which is known to compete with Ca^{2+} for transport into mitochondria via the Ca^{2+} uniporter, and hence inhibits mitochondrial Ca^{2+} uptake (9–13)). Therefore, the apparent activity of the uniporter in either cardiac or liver mitochondria could not be estimated with confidence from this data, without additional knowledge of the chemical constituents of the mitochondrial preparations.

Analysis of different kinetic data with Model 1 and Model 2 under Case 2 showed that the model parameter values are readjusted to provide similar fits of the model to the three independent data sets. Nevertheless, there are consistently similar trends in the estimated model parameter values between different data sets (e.g., $K_e^0 \ll K_x^0$ and $k_{in}^0 \gg k_{out}^0$) (Table 1). The estimated values of the biophysical parameters α_e, α_x, β_e and β_x did not differ significantly between different models under any particular case (Table 1). The estimated value of α_e was consistently negligible and that of α_x was negative; so we fixed $\alpha_e = 0$ and estimated α_x along with the two most sensitive biophysical parameters β_e and β_x. The estimates of α_e, α_x, β_e and β_x corresponding to Case 2 that provided the best fit of the models to the data suggest that 1), since α_x is negative, the charge distribution on the uniporter during Ca^{2+} binding to the uniporter and Ca^{2+} translocation via the uniporter is not linearly decreasing along the reaction coordinate (i.e., the direction of Ca^{2+} translocation from outside to inside of the uniporter), and 2), since $\beta_e \approx 0.26$ and $\beta_e \approx 0.96$, the free-energy barrier that impedes the Ca^{2+} translocation, is not symmetric. These estimates result in stiff gradients in Ca^{2+} uptake profiles with respect to the membrane potential $\Delta\Psi$, as depicted in Fig. 3, *B*, *D*, and *F*, and Fig. 4, *B*, *D*, and *F* (*right panels*).

DISCUSSION

The major contributions of our theoretical study is the detailed characterization of the kinetics of mitochondrial Ca^{2+} uniporter, which is the primary influx pathway for Ca^{2+} in respiring (energized) mitochondria, and hence is a key regulator of mitochondrial Ca^{2+}. This characterization is done based on a biophysically-based, mechanistic mathematical model that is compared to several independent experimental data sets on mitochondrial Ca^{2+} uptake in the literature. Our model differs from the previous attempts (16,21,22) in that it is thermodynamically balanced and adequately describes the independent experimental data sets of Scarpa and co-workers (10,11) as well as Gunter and co-workers (6,18) on Ca^{2+} influx through the Ca^{2+} uniporter in energized

mitochondria isolated from rat heart and rat liver measured under varying experimental conditions. Although there is no direct experimental evidence regarding the structure and composition of the mitochondrial Ca^{2+} uniporter functional unit and the mechanisms for Ca^{2+} binding to the uniporter, our model is consistent with the hypothesis of Scarpa and co-workers (10,11) regarding the presence of at least two Ca^{2+} binding sites on the uniporter for uniporter-mediated Ca^{2+} translocation across the IMM. Alternatively, by considering a single Ca^{2+} binding site on the uniporter, we were not able to fit the resulting model to the experimental data of Scarpa and co-workers.

The mitochondrial Ca^{2+} uniporter model developed here is able to explain the experimental data of Gunter and co-workers (6,18) on mitochondrial Ca^{2+} uptake as a function of membrane potential $\Delta\Psi$ (Fig. 3 *F*) without introducing the nonphysical assumptions of previous models (6,16). Specifically, these models have introduced an offset potential $\Delta\Psi^*$ ($\approx$ 91 mV) and flux expressions that appropriate for potential measured relative to this offset potential. These kinetic models of the uniporter were justified based on the explanation that the electrical potential across the uniporter may not fall to zero concomitantly with the bulk membrane potential, perhaps because of fixed charges producing electric field gradients localized to the uniporter. However, such models cannot be reconciled with measurements of bulk Ca^{2+} movement between the matrix and extra-matrix buffer space. The current biophysical model of the uniporter is able to account for the observed kinetic data based on a mechanistic formulation that is thermodynamically feasible. In doing this the singularity that occurs at $\Delta\Psi = \Delta\Psi^* \approx 91$ mV in previous models does not exist in the current model.

The analysis of the two kinetic models of the mitochondrial Ca^{2+} uniporter developed here shows that for these models to fit the available kinetic data on mitochondrial Ca^{2+} uptake, the dissociation constants associated with the binding of external and internal Ca^{2+} to the uniporter in the absence of electric field (i.e., $\Delta\Psi = 0$) has to be asymmetric (i.e., K_e^0 and K_x^0 has to be distinct; K_e^0 is found to be an order of magnitude higher than K_x^0; Table 1). The estimates of biophysical parameters α_e, α_x, β_e and β_x corresponding to the this condition (Case 2; K_e^0 and K_x^0 are distinct) that provide the best fit of the model to the available kinetic data suggest that 1), the charge distribution on the uniporter during Ca^{2+} binding to the uniporter and Ca^{2+} translocation via the uniporter is not linearly decreasing along the direction of Ca^{2+} translocation from outside to inside of the uniporter (since α_x is estimated to be negative), and 2), the free-energy barrier that impedes the Ca^{2+} translocation is not symmetric (since $\beta_e \approx 0.26$ and $\beta_e \approx 0.96$).

Based on our model analysis of the available kinetic data, we were not able to distinguish between the two related versions of the kinetic model for the uniporter. The available experimental data are mostly initial (or pseudo steady state) Ca^{2+} influx rates via the uniporter. In these experiments, $[Ca^{2+}]_x$ (intra-mitochondrial Ca^{2+}) was typically negligible compared to $[Ca^{2+}]_e$ (amount of Ca^{2+} added to the extra-mitochondrial buffer medium) for various initial Ca^{2+} influx measurements. As a result, this experimental data was not enough to fully identify the kinetic mechanisms associated with the binding steps of Ca^{2+} with the uniporter. Since both kinetic models predict all the available experimental data equally well, neither versions of the kinetic model can be excluded.

Our Ca^{2+} uniporter model simulations show that as the mitochondrial inner membrane depolarizes (i.e., as the membrane potential $\Delta\Psi$ decreases), the mitochondrial Ca^{2+} uptake as well as the maximum uptake velocity and saturating Ca^{2+} concentration decreases. Furthermore, the gradient of the decrease becomes smaller and smaller with

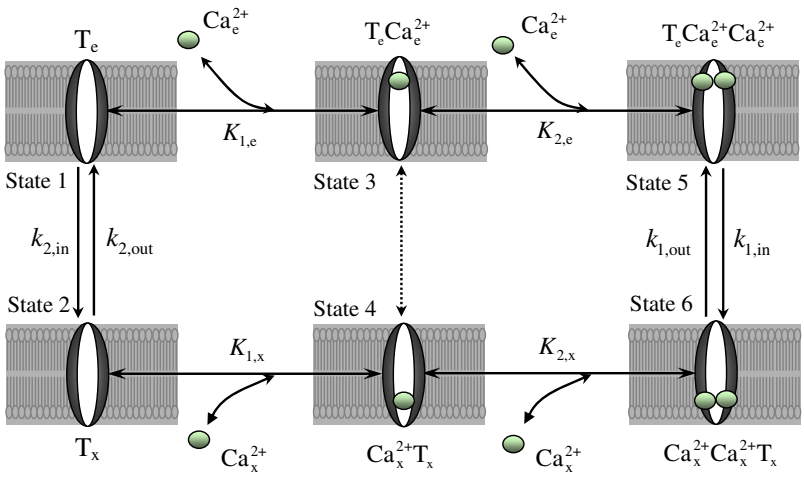

FIGURE 5 Another possible 6-states kinetic mechanism of Ca^{2+} transport into mitochondria via the Ca^{2+} uniporter. The unbound uniporter (T) is assumed to have two binding sites for Ca^{2+} and present in two conformal states (T_e and T_x, *State 1* and *State 2*). The binding sites in T_e and T_x face to the external and internal sides of the IMM, respectively. The ionized free Ca^{2+} from the external side of the IMM (Ca_e^{2+}) cooperatively binds to the unbound uniporter (T_e, *State 1*) in two steps to form the complex $T_e.Ca_e^{2+}.Ca_e^{2+}$(*State 5*) which then undergoes conformational changes (or flips upside down) to form the complex $Ca_x^{2+}.Ca_x^{2+}.T_x$(*State 6*). The complex $Ca_x^{2+}.Ca_x^{2+}.T_x$ in the internal side of the IMM goes through the reverse process; it dissociates in two steps to form the unbound uniporter (T_x, *State 2*) and ionized free Ca^{2+}. The unbound uniporter T_x then undergoes conformational changes (or flips upside down) to the original state T_e. ($K_{1,e}$, $K_{1,x}$) and ($K_{2,e}$, $K_{2,x}$) are the two pairs of dissociation (binding) constants for the two step uniporter binding reactions with the external and internal Ca^{2+}. The transport of Ca^{2+} via the Ca^{2+} uniporter is limited by the rate constants $k_{1,in}$, $k_{1,out}$, $k_{2,in}$, and $k_{2,out}$ which are dependent on the membrane potential $\Delta\Psi$.

each subsequent decrease of the membrane potential $\Delta\Psi$, as depicted in Fig. 3, *B, D*, and *F*, and Fig. 4, *B, D*, and *F* (*right panels*). This is consistent in part with the experimental observations of Gunter and co-workers (6,18) (Fig. 3 *F*). As shown by the model simulations in Fig. 4 *F*, the Ca^{2+} uptake in cardiac mitochondria saturates beyond $[Ca^{2+}]_e = 100\ \mu M$. Though precise experimental data were not available to validate these simulations, the Ca^{2+} uptake kinetics are similar to those of the Ca^{2+} currents observed in the studies of Kirichok et al. (23) using patch-clamp techniques in mitoplasts isolated from cardiac mitochondria. However, their reported value $K_m = 19$ mM is significantly higher compared to the values obtained here ($K_m < 100\ \mu M$ for cardiac mitochondria and $K_m < 50\ \mu M$ for liver mitochondria). Therefore, we were unable to successfully compare our model simulations to the experimental data of Kirichok et al. (23) relating the Ca^{2+} current and membrane potential $\Delta\Psi$. Using the assumption that the mitochondrial Ca^{2+} uniporter is a highly selective ion channel permeable only to Ca^{2+}, Jafri and co-workers (21,22) were able to simulate the data of Kirichok et al. (23) using a simple kinetic model of the uniporter based on the Goldman-Hodgkin-Katz equation (reasonable as the K_m is very large; $K_m = 19$ mM). Therefore, the Jafri et al. model is able to explain the data of Kirichok et al. from mitoplasts, whereas our model explains the independent data sets of Scarpa et al. and Gunter et al. from intact mitochondria. Neither model can simultaneously explain all of these data sets. Since the Jafri et al. model is developed from data from patch-clamp mitoplasts and our model is developed from data from intact mitochondria, the differences between these models may reflect fundamentally different behavior of the uniporter in the experimental preparations. A comparison between this model and previous models of the uniporter is given in the Supporting Material.

Current knowledge of cardiac myocytes Ca^{2+} handling suggests the existence of intracellular Ca^{2+} sub-domains (junctional cleft or sub membrane space, where higher Ca^{2+} or Na^+ concentrations, compared to the average Ca^{2+} and Na^+ levels in the cytoplasm, may develop during the cell excitation) (32). These Ca^{2+} sub-domains are believed to be essential in some critical aspects of the cell signaling and cell cycling. Consequently, the mitochondrial population situated near these Ca^{2+} sub-domains is expected to have different behavior (e.g., higher Ca^{2+} uptake; also possibly increased redox states and increased respiration) compared to a mitochondrial population that is far away from the Ca^{2+} sub-domains. Therefore, this biophysical model of the mitochondrial Ca^{2+} uniporter will form the basis for constructing biophysically-based, integrated models of mitochondrial Ca^{2+} handling and bioenergetics (by integrating the Ca^{2+} uniporter model to our existing models of mitochondrial tricarboxylic acid cycle, oxidative phosphorylation, cation handling, and electrophysiology (15,33)), which may be helpful in understanding the mechanisms by which Ca^{2+} plays a role in mediating signaling pathways and modulating mitochondrial energy metabolism, both locally as well as over the whole cell.

To summarize, we have developed a theoretical model for the kinetics of the mitochondrial Ca^{2+} uniporter based on a six-state catalytic binding and interconversion mechanism (Fig. 1). In this scheme, the unbound uniporter (*T*) is assumed to have only one conformational state. The fully bound uniporter (T-2Ca^{2+}) is assumed to undergo a conformational change ($T\,Ca_e^{2+}Ca_e^{2+} \leftrightarrow Ca_x^{2+}Ca_x^{2+}T$) transporting Ca^{2+} from the external (cytosolic) side to the internal (matrix) side of the IMM. The model is effective and convenient because it explains the available experimental data on the kinetics of mitochondrial Ca^{2+} uptake with a minimum number of adjustable parameters. However, alternate kinetic models are possible. Consider, for example, the kinetic mechanism illustrated in Fig. 5 in which the unbound uniporter (*T*) is assumed to have two conformational states (T_x and T_e) depending on the orientation and position of the Ca^{2+} binding sites on the external or internal sites of the IMM, in addition to the two conformational states of the fully bound uniporter ($T\,Ca_e^{2+}Ca_e^{2+}$ and $Ca_x^{2+}Ca_x^{2+}T$). The model involves two additional rate constants for this conformational change which depend on the membrane potential $\Delta\Psi$ depending on the charge on the unbound uniporter (which is not well known). Applying this model will involve a greater number of adjustable parameters than the model presented here.

APPENDIX: GLOSSARY OF VARIABLES

Variables	Definition	Units
$[Ca^{2+}]_e$	Extra-mitochondrial concentration of ionized (free) Ca^{2+}	M
$[Ca^{2+}]_x$	Intra-mitochondrial concentration of ionized (free) Ca^{2+}	M
$K_{1,e}, K_{1,x}, K_{2,e}, K_{2,x}$	Dissociation constants of $T\,Ca_e^{2+}$ and $Ca_x^{2+}T$ (1st binding step) and $T\,Ca_e^{2+}Ca_e^{2+}$ and $Ca_x^{2+}Ca_x^{2+}T$ (2nd binding step)	M
$K_e,\ K_x$	$K_e = \sqrt{K_{1,e}K_{2,e}}$ and $K_x = \sqrt{K_{1,x}K_{2,x}}$ (Model-1) $K_e = K_{1,e} = K_{2,e}$ and $K_x = K_{1,x} = K_{2,x}$ (Model-2)	M
$K^0_{1,e}, K^0_{1,x}, K^0_{2,e}, K^0_{2,x}$	$K^0_{1,e} = K_{1,e}(\Delta\Psi = 0) = \exp(-\Delta\mu^0_{1,e}/RT);\ K^0_{1,x} = K_{1,x}(\Delta\Psi = 0) = \exp(-\Delta\mu^0_{1,x}/RT)$ $K^0_{2,e} = K_{2,e}(\Delta\Psi = 0) = \exp(-\Delta\mu^0_{2,e}/RT);\ K^0_{2,x} = K_{2,x}(\Delta\Psi = 0) = \exp(-\Delta\mu^0_{2,x}/RT)$	M

APPENDIX Continued

Variables	Definition	Units
K_e^0, K_x^0	$K_e^0 = \sqrt{K_{1,e}^0 K_{2,e}^0}$ and $K_x^0 = \sqrt{K_{1,x}^0 K_{2,x}^0}$ (Model-1) $K_e^0 = K_{1,e}^0 = K_{2,e}^0$ and $K_x^0 = K_{1,x}^0 = K_{2,x}^0$ (Model-2)	M kJ/mol
$\Delta\mu_{1,e}$, $\Delta\mu_{1,x}$, $\Delta\mu_{2,e}$, $\Delta\mu_{2,x}$	Changes in Gibb's free-energy for the dissociation of T Ca_e^{2+}, Ca_x^{2+}T, T $Ca_e^{2+}Ca_e^{2+}$, and $Ca_x^{2+}Ca_x^{2+}$T	
$\Delta\mu_{1,e}^0$, $\Delta\mu_{1,x}^0$, $\Delta\mu_{2,e}^0$, $\Delta\mu_{2,x}^0$	The corresponding standard changes in Gibb's free energy: $\Delta\mu_{1,e}^0 = -RT\ln(K_{1,e}^0)$; $\Delta\mu_{1,x}^0 = -RT\ln(K_{1,x}^0)$; $\Delta\mu_{2,e}^0 = -RT\ln(K_{2,e}^0)$; $\Delta\mu_{2,x}^0 = -RT\ln(K_{2,x}^0)$	kJ/mol nmol/mg/sec
k_{in}, k_{out}, k_{in}^0, k_{out}^0	Forward and reverse rate constants for the conformational change reaction: T $Ca_e^{2+}Ca_e^{2+} \leftrightarrow Ca_x^{2+}Ca_x^{2+}$T ($k_{in}^0 = k_{in}(\Delta\Psi = 0)$; $k_{out}^0 = k_{out}(\Delta\Psi = 0)$)	
ΔG_{in}, ΔG_{out}, ΔG_{in}^0, ΔG_{out}^0	Heights of the free-energy barrier for the forward and reverse rate constants: $\Delta G_{in}^0 = \Delta G_{in}(\Delta\Psi = 0)$; $\Delta G_{out}^0 = \Delta G_{out}(\Delta\Psi = 0)$(Fig. 2B)	kJ/mol
K_{eq}	Equilibrium constant for trans-membrane Ca^{2+} transport via the Ca^{2+} uniporter	unitless
[T]	Concentration of the unbound (free) transporter (Ca^{2+} uniporter)	M
$[T]_{tot}$	Total concentration of the transporter (Ca^{2+} uniporter)	M
D, D_1, D_2	Binding polynomial for the Ca^{2+} and Ca^{2+} uniporter binding (Eq. 5)	unitless
X_{Uni}, J_{Uni}	Activity of the Ca^{2+} uniporter and the corresponding rate of Ca^{2+} transport via the Ca^{2+} uniporter: $X_{Uni} = [T]_{tot}.k_{out}^0$	nmol/mg/sec
$\Delta\Psi$	Electrostatic potential difference across the IMM	mV
$\Delta\Phi$	Nondimensional electrostatic potential difference across the IMM: $\Delta\Phi = Z_{Ca}F\Delta\Psi/RT$ (where F, R, T, and Z_{Ca} are defined in Table 1)	unitless
α_e (α_x)	Ratio of the potential difference between Ca^{2+} bound at the site of uniporter facing the external (internal) side of the IMM and Ca^{2+} in the bulk phase to the total IMM potential $\Delta\Psi$ (Fig. 2 *A*)	unitless
β_e (β_x)	Displacement of external or internal Ca^{2+} (State I or State III) from the coordinate of maximum potential barrier (State II) (Fig. 2 *A*)	unitless

SUPPORTING MATERIAL

A table, equations, and figures are available at http://www.biophysj.org/biophysj/supplemental/S0006-3495(08)00111-2.

This research was supported by the grants R01-HL072011 (D.A.B.) from the National Institute of Health and SDG-0735093N (R.K.D.) from the American Heart Association.

REFERENCES

1. Bernardi, P. 1999. Mitochondrial transport of cations: channels, exchangers, and permeability transition. *Physiol. Rev.* 79:1127–1155.
2. Brookes, P. S., Y. Yoon, J. L. Robotham, M. W. Anders, and S. S. Sheu. 2004. Calcium, ATP, and ROS: a mitochondrial love-hate triangle. *Am. J. Physiol. Cell Physiol.* 287:C817–C833.
3. Duchen, M. R. 1999. Contributions of mitochondria to animal physiology: from homeostatic sensor to calcium signalling and cell death. *J. Physiol.* 516:1–17.
4. Duchen, M. R. 2000. Mitochondria and Ca^{2+} in cell physiology and pathophysiology. *Cell Calcium.* 28:339–348.
5. Duchen, M. R. 2000. Mitochondria and calcium: from cell signalling to cell death. *J. Physiol.* 529:57–68.
6. Gunter, T. E., and D. R. Pfeiffer. 1990. Mechanisms by which mitochondria transport calcium. *Am. J. Physiol.* 258:C755–C786.
7. Gunter, T. E., K. K. Gunter, S. S. Sheu, and C. E. Gavin. 1994. Mitochondrial calcium transport: physiological and pathological relevance. *Am. J. Physiol.* 267:C313–C339.
8. O'Rourke, B., S. Cortassa, and M. A. Aon. 2005. Mitochondrial ion channels: gatekeepers of life and death. *Physiology (Bethesda).* 20:303–315.
9. Crompton, M., E. Sigel, M. Salzmann, and E. Carafoli. 1976. A kinetic study of the energy-linked influx of Ca^{2+} into heart mitochondria. *Eur. J. Biochem.* 69:429–434.
10. Scarpa, A., and P. Graziotti. 1973. Mechanisms for intracellular calcium regulation in heart. I. Stopped-flow measurements of Ca^{2+} uptake by cardiac mitochondria. *J. Gen. Physiol.* 62:756–772.
11. Vinogradov, A., and A. Scarpa. 1973. The initial velocities of calcium uptake by rat liver mitochondria. *J. Biol. Chem.* 248:5527–5531.
12. McCormack, J. G., H. M. Browne, and N. J. Dawes. 1989. Studies on mitochondrial Ca^{2+}-transport and matrix Ca^{2+} using fura-2-loaded rat heart mitochondria. *Biochim. Biophys. Acta.* 973:420–427.
13. Wan, B., K. F. LaNoue, J. Y. Cheung, and R. C. Scaduto, Jr. 1989. Regulation of citric acid cycle by calcium. *J. Biol. Chem.* 264:13430–13439.
14. Gursahani, H. I., and S. Schaefer. 2004. Acidification reduces mitochondrial calcium uptake in rat cardiac mitochondria. *Am. J. Physiol. Heart Circ. Physiol.* 287:H2659–H2665.
15. Dash, R. K., and D. A. Beard. 2008. Analysis of cardiac mitochondrial Na^+/Ca^{2+} exchanger kinetics with a biophysical model of mitochondrial Ca^{2+} handling suggests a 3:1 stoichiometry. *J. Physiol.* 586:3267–3285.
16. Magnus, G., and J. Keizer. 1997. Minimal model of β-cell mitochondrial Ca^{2+} handling. *Am. J. Physiol.* 273:C717–C733.

17. Magnus, G., and J. Keizer. 1998. Model of β-cell mitochondrial calcium handling and electrical activity. II. Mitochondrial variables. *Am. J. Physiol.* 274:C1174–C1184.

18. Wingrove, D. E., J. M. Amatruda, and T. E. Gunter. 1984. Glucagon effects on the membrane potential and calcium uptake rate of rat liver mitochondria. *J. Biol. Chem.* 259:9390–9394.

19. Cortassa, S., M. A. Aon, E. Marban, R. L. Winslow, and B. O'Rourke. 2003. An integrated model of cardiac mitochondrial energy metabolism and calcium dynamics. *Biophys. J.* 84:2734–2755.

20. Miyata, H., H. S. Silverman, S. J. Sollott, E. G. Lakatta, M. D. Stern, et al. 1991. Measurement of mitochondrial free Ca2+ concentration in living single rat cardiac myocytes. *Am. J. Physiol.* 261:H1123–H1134.

21. Nguyen, M. H., and M. S. Jafri. 2005. Mitochondrial calcium signaling and energy metabolism. *Ann. N. Y. Acad. Sci.* 1047:127–137.

22. Nguyen, M. H., S. J. Dudycha, and M. S. Jafri. 2007. The effects of Ca^{2+} on cardiac mitochondrial energy production is modulated by Na^{+} and H^{+} dynamics. *Am. J. Physiol. Cell Physiol.* 292:2004–2020.

23. Kirichok, Y., G. Krapivinsky, and D. E. Clapham. 2004. The mitochondrial calcium uniporter is a highly selective ion channel. *Nature.* 427:360–364.

24. Fall C. P., Wagner J., and Marland E., editors. (2002). Computational Cell Biology. Springer, New York.

25. Keener, J. P., and J. Sneyd. 1998. Mathematical Physiology. Springer, New York.

26. Lauger, P. 1973. Ion transport through pores: a rate-theory analysis. *Biochim. Biophys. Acta.* 311:423–441.

27. Lauger, P., and B. Neumcke. 1973. Theoretical analysis of ion conductance in lipid bilayer membranes. *Membranes.* 2:1–59.

28. Woodbury, J. W. 1971. Eyring rate theory model of the current-voltage relationship of ion channels in excitable membranes. *In* Chemical Dynamics: Papers in Honor of Henry Eyring. J. Hirschfelder, editor. John Wiley and Sons Inc., New York.

29. Ussing, H. H. 1949. Transport of ions across cellular membranes. *Physiol. Rev.* 29:127–155.

30. Beard, D. A., and H. Qian. 2007. Relationship between thermodynamic driving force and one-way fluxes in reversible processes. *PLoS ONE.* 2:e144.

31. Metelkin, E., I. Goryanin, and O. Demin. 2006. Mathematical modeling of mitochondrial adenine nucleotide translocase. *Biophys. J.* 90:423–432.

32. Michailova, A., and A. McCulloch. 2001. Model study of ATP and ADP buffering, transport of Ca^{2+} and Mg^{2+}, and regulation of ion pumps in ventricular myocyte. *Biophys. J.* 81:614–629.

33. Wu, F., F. Yang, K. C. Vinnakota, and D. A. Beard. 2007. Computer modeling of mitochondrial tricarboxylic acid cycle, oxidative phosphorylation, metabolite transport, and electrophysiology. *J. Biol. Chem.* 282:24525–24537.